PROCEEDINGS OF SPIE

SPIEDigitalLibrary.org/conference-proceedings-of-spie

Active health monitoring of TN32 dry cask using a scaled down model

Roshan Joseph, Stephen Howden, Bin Lin, Lingyu Yu, Victor Giurgiutiu

Roshan Joseph, Stephen Howden, Bin Lin, Lingyu Yu, Victor Giurgiutiu, "Active health monitoring of TN32 dry cask using a scaled down model ," Proc. SPIE 10600, Health Monitoring of Structural and Biological Systems XII, 106000B (27 March 2018); doi: 10.1117/12.2297278

SPIE.

Event: SPIE Smart Structures and Materials + Nondestructive Evaluation and Health Monitoring, 2018, Denver, Colorado, United States

Active health monitoring of TN32 dry cask using a scaled down model

Roshan Joseph, Stephen Howden, Bin Lin, Lingyu Yu, Victor Giurgiutiu
Department of Mechanical Engineering, University of South Carolina, Columbia, USA

ABSTRACT

TN32 casks are multi-layer cylindrical structures used for storage of nuclear spent fuel. The National Center for Physical Acoustics at the University of Mississippi has manufactured a scaled down model of the TN32 cask. To identify the most relevant nondestructive evaluation parameters, which will be useful while doing experiments on real TN32 casks, a series of experiments have been conducted on TN32 cask model. This paper discusses the data analysis of the experiments conducted on the cask model and the conclusions based on those experiments. Elastodynamic waves are generated in the cask model by pencil lead break and hammer hit excitation and the waves in the cask at certain locations are sensed using piezoelectric wafer active sensors (PWAS). The waveforms and frequency spectrums of waveforms arriving at PWAS are studied. There are two types of joints on the cask model: structures joined using adhesives and structures joined using press fit. The effects of various joints in the structure on elastodynamic wave propagation are also studied. Pitch catch experiments on the cask was also done using in plane excitation using PWAS. The most sensitive frequency for the cask model was identified from the frequency response spectrum obtained from a wide band chirp excitation. The influence of various joints on the frequency response spectrum is also studied. Analytical modeling of cask geometry for a given excitation is done using Normal Mode Expansion (NME) technique. Prediction of wave propagation through the scaled down model is done based on the theoretical expression derived.

Keywords: Acoustic emission, TN32 cask, active structural health monitoring, wave propagation through thick shells, wave propagation through joints.

1. INTRODUCTION

TN32 casks are multi-layer cylindrical structures used for storage of nuclear spent fuel. This paper aims at structural integrity investigation of a scaled down model of TN32 cask for benefitting towards the experiments on real TN32 cask. For theoretical understanding of guided wave propagation in the scaled down cask model, predictive modeling of guided wave propagation in the present scaled down hollow cylinder structure is conducted using semi analytical finite element (SAFE) approach and through comparison of the predictions with experimentally obtained signals. This paper also aims a health monitoring of TN32 scaled down model by using pencil lead break as well as hammer hit wave propagation sources.

Theoretical development of guided wave propagation in hollow cylinders were well studied in the past century. Flexural guided waves in pipes have been known for decades. Gazis studied exact analytical model for guided wave propagation in hollow cylinder [1]. He showed that there exists an infinite number of normal modes, including axisymmetric modes and non-axisymmetric modes in an elastic hollow cylinder. Each mode has its own characteristics such as phase velocity, group velocity etc. He obtained the general solution of harmonic waves propagating in an infinite long hollow cylinder. Normal mode expansion (NME) of hollow cylinder modes for a force excitation was first studied by Ditri et al.[2]. He derived a closed form solution for normal mode expansion coefficients for hollow cylinder modes due to a force excitation. The excitation and propagation of non-axisymmetric longitudinal waves by using NME with different sources are studied by Li et al [3]. The angular profile due to such an excitation is obtained by constructive and destructive interference of amplitude factors of every excited mode. Sun et al [4] studied flexural torsional wave mechanics and focusing by NME. Even though active structural health monitoring using PWAS in hollow cylindrical structures is not well explored as in plate like structures[5][6][7]. Also passive health monitoring in hollow cylindrical structures is also not explored well as in plate[8][9][10][11]

For generation of axisymmetric modes different kinds of generation methods are widely used. Many uses comb transducer as well as dry couples normal beam transducer for generation of axisymmetric guided wave generation in hollow cylinders[12][13]. A transducer array made of series of normal beam transducers can also be used for axisymmetric guided wave generation[14]. When only a portion of cylinder might be accessible for source loading, non-axisymmetric guided waves will be generated. In such circumstances, acoustic field is more complicated and energy distribution of the wave propagation needs to be known in order to evaluate the guided wave inspection ability and to perform frequency and angle tuning [2].

Health Monitoring of Structural and Biological Systems XII, edited by Tribikram Kundu, Proc. of SPIE
Vol. 10600, 106000B · © 2018 SPIE · CCC code: 0277-786X/18/$18 · doi: 10.1117/12.2297278

Semi- analytical finite element method (SAFE) is used for guided wave calculations in hollow cylinders [15]. Long range calculations can be done with little computational time and memory with SAFE method since it does not require discretization in the wave propagation direction. Early works of SAFE method was done by Nelson, et al [16]. They successfully formulated SAFE wave equations for elastic layered orthotropic cylinders and plates by means of mono dimensional cross- section interpolation.

Afterwards, the SAFE method has been effectively used to model guided wave propagation in anisotropic composite cylinders [17], laminated composite plates [18], wedges[19], rails[20], functionally graded cylinders[21], piezoelectric plates [22], laminated piezoelectric cylinders[23], channel beams[24]. SAFE approach for accounting viscoelastic materials is also developed [25][26].

This paper is divided in to following sections. Section 2 discusses on geometry and key locations of the hollow cylinder structure under investigation. Section 3 discusses on SAFE-NME theoretical development and numerical simulation for excitation due to a PWAS transducer. A comparison of experimentally obtained signal and theoretically prediction is done in section 3.2. Section 4 is on effect of various types of joints on wave propagation in the structure. AE excitations are given in to the structure at various excitation locations (as explained in section 2) and signals detected at various locations are analyzed in this section. Section 4 is an investigation of the frequency response of the structure due to an in-plane chirp excitation in the cylinder using PWAS.

2. EXPERIMENTAL SETUP

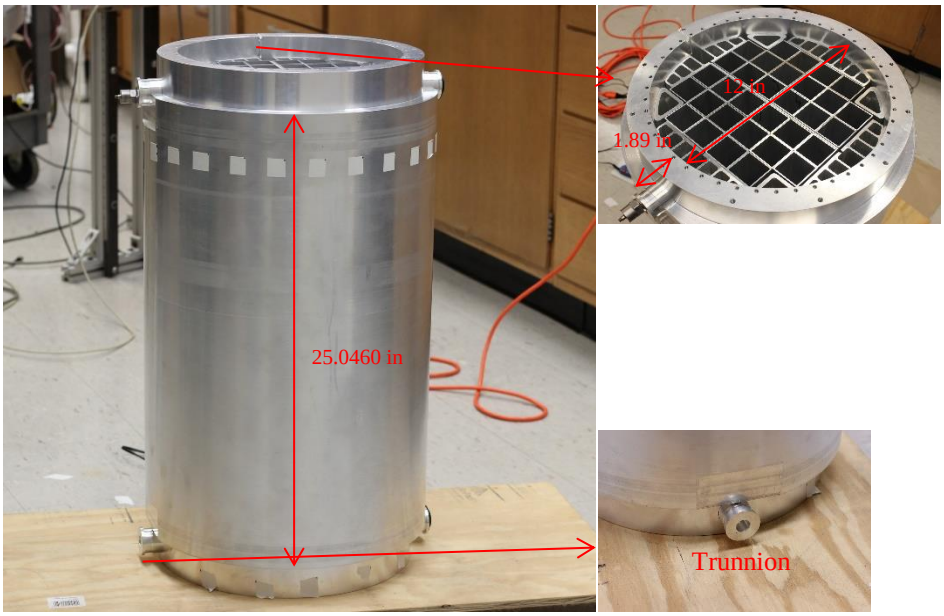

Figure 1 Hollow cylinder geometry with dimensions

Figure 1 represents the hollow cylinder cask geometry manufactured by The National Center for Physical Acoustics at the University of Mississippi which is used for experimental investigation. The cask is manufactured with Aluminum 2024 material. It has a height of approximately 29” and diameter of 15”.Its main component is a cylindrical wall of thickness 1.89” attached with 2 trunnions on top and 2 on the bottom. The trunnions are attached to the cylinder by press fit, which provides a discontinuity for wave propagation. The effect of press fit joints on wave propagation will be discussed in the section 4. The basket for carrying the spent fuel rods is inserted in to the hollow cylinder through basket guides attached to the inside of cylinder. Basket guides are attached inside the cylinder by bolted and adhesive joints.

Excitation is given at various locations in the hollow cylinder by using AE sources such as hammer hit and pencil lead break and through active excitation sing PWAS. The key locations for excitations and sensor positions are shown in Figure 2. Major exciter and receiver locations in the experimental set up are BG1, BG2, BG3 (BG stands for basket guide, since these locations are on the basket guide), T1, T2, T3, T4 (T stands for trunnion, since these locations are on the four trunnions), TF1, TF2 (TF stands for trunnion face. These are small flat faces near trunnion 1 and 2) S1, S2, S3 and SG5 (S stands for surface, since these locations are on the surface of the cylinder.

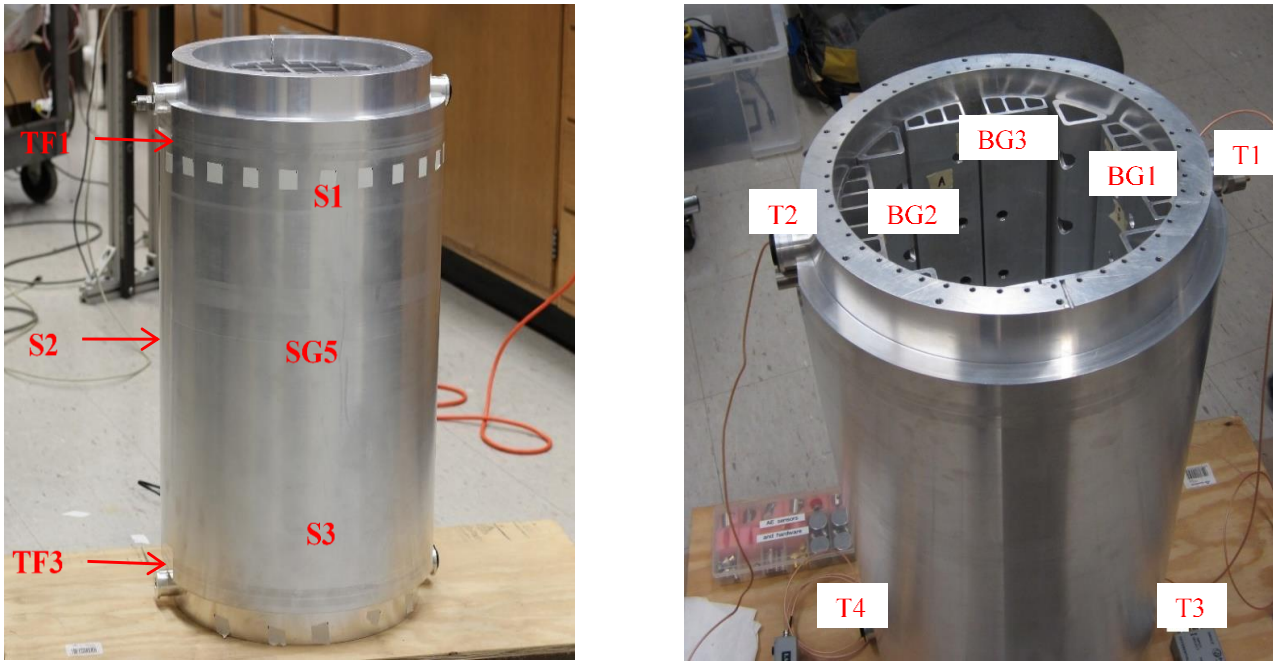

(a) (b)

Figure 2 Key locations for sensor placement and excitation on hollow cylinder

Both active and passive excitations are given at various locations in the cylinder and signals are received using various receiver transducers installed at T1, T2, T3, T3, TF1 and TF2. We have used wsα, R15α and PWAS for receiving signals. Wsα sensor is a wide band sensor. This sensor is sensitive to a wide band of frequencies approximately ranging between 30 kHz to 1 MHz. Whereas R15α is a resonant type sensor with a resonant frequency of 150 kHz. This means, the sensor is highly sensitive to 150 kHz frequency. The signals received using wsα, R15α and PWAS are amplified using a pre-amplifier before sending it to MISTRAS AE system for analysis.

3. SEMI ANALYTICAL FINITE ELEMENT (SAFE)- NORMAL MODE EXPANSIO (NME) FOR PREDICTION OF LAMB WAVE PROPAGATION IN HOLLOW CYLINDERS

3.1 Theoretical formulation

For prediction of lamb wave modes due to PWAS excitation, semi analytical finite element (SAFE) approach is adopted and formulated. SAFE adopts harmonic domain $e^{i(\xi x-\omega t)}$ to describe the wave behavior in the wave propagation direction, where x is the wave propagation direction, ξ represents the wave number, ω is the radial frequency and t is the time. Finite element discretization of the SAFE method takes place at the cross section of the wave guide.
The displacement field solution for a non-homogeneous condition where loading $F \neq 0$ can be obtained by using normal mode expansion method. The displacement field will be the summation of the orthogonal modes as following

$$U = \sum_{m=1}^{2M} U_m \Phi_m \tag{1}$$

Where, U_m is the normal mode expansion coefficient given as

$$U_m = \frac{\hat{V}_m^L P}{(\xi_m - \xi)\hat{V}_m^L P \hat{V}_m^R}, \quad \xi \neq \xi_m, m = 1, 2, ..., 2M \tag{2}$$

And Φ_m is the mode shape vector.

For obtaining the displacement field in the physical domain from the displacement field in wavenumber domain in eq.(1) , we take inverse Fourier transform with respect to wavenumbers, ξ_x, ξ_y

$$u(x,y,\omega)=\frac{1}{4\pi^2}\int_{-\infty}^{+\infty}\int_{-\infty}^{+\infty}\sum_{m=1}^{M}\frac{\hat{V}_m^L P}{(\xi_m-\xi)\hat{V}_m^L P\hat{V}_m^R}\Phi_m e^{i(\xi_x x+\xi_y y)}d\xi_x d\xi_y \tag{3}$$

Changing from Cartesian to cylindrical coordinate system, we get

$$u(r,\theta,\omega)=\frac{1}{4\pi^2}\int_{-\infty}^{+\infty}\int_{-\infty}^{+\infty}\sum_{m=1}^{M}\frac{\hat{V}_m^L P}{(\xi_m-\xi)\hat{V}_m^L P\hat{V}_m^R}\Phi_m e^{i\xi(x\cos\theta+y\sin\theta)}\xi d\xi d\theta \tag{4}$$

The excitation due to an ideally bonded PWAS is expressed as the traction acting at the circumference of a circular PWAS of radius a . The axisymmetric shear stress acting is shown in the following figure.

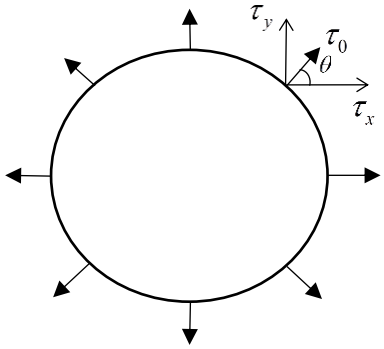

Figure 3 Traction acting on the surface of the plate due to PWAS excitation

For a circular PWAS excitation, the forcing functions τ_x , τ_y and their Fourier transform are expresses as following respectively

$$\begin{aligned}
\tau_x &= \tau_0\delta(r-a)\cos\theta \\
\tau_y &= \tau_0\delta(r-a)\sin\theta \\
\bar{\tau}_x &= -ia\tau_0 J_1(\xi a)\cos\theta \\
\bar{\tau}_y &= -ia\tau_0 J_1(\xi a)\sin\theta
\end{aligned} \tag{5}$$

The integral in eq.(4) could be singular at points corresponding to real roots of Rayleigh-Lamb equation or roots of shear horizontal waves or both after substituting $\bar{\tau}_x$ and $\bar{\tau}_y$. The excitation $\bar{\tau}_x$ will correspond to excitation for propagating Lamb wave corresponding to the roots of Rayleigh- Lamb equation and $\bar{\tau}_y$ will correspond to the excitation for horizontally polarized shear horizontal (SH) waves. Since in this work, we are only considering propagation of Lamb wave predictive modeling, we need to consider only $\bar{\tau}_x$ excitation. Hence, excitation for Lamb wave propagation due to PWAS, or the component P in eq. (4) is written as

$$P=\begin{bmatrix}0\\ \hat{F}\end{bmatrix} \tag{6}$$

Where,

$$\hat{F} = \begin{bmatrix} -ia\tau_0 J_1(\xi a)\cos\theta \\ 0 \\ . \\ . \\ 0 \end{bmatrix} = \begin{bmatrix} 1 \\ 0 \\ . \\ . \\ 0 \end{bmatrix} (-ia\tau_0 J_1(\xi a)\cos\theta) = \hat{F}_1(-ia\tau_0 J_1(\xi a)\cos\theta) \tag{7}$$

Hence, we write,

$$P = P_1(-ia\tau_0 J_1(\xi a)\cos\theta) = P_1(-ia\tau_0 J_1(\xi a)\,{}^{\xi_x}\!/_{\xi}) \tag{8}$$

Where,

$$P_1 = \begin{bmatrix} 0 \\ \hat{F}_1 \end{bmatrix} \tag{9}$$

Substituting eq.(9) into eq.(4) we get,

$$u(r,\theta,\omega) = \frac{1}{4\pi^2}\int_{-\infty}^{+\infty}\int_{-\infty}^{+\infty}\sum_{m=1}^{M}\frac{\hat{V}_m^L P_1}{(\xi_m-\xi)\hat{V}_m^L P\hat{V}_m^R}\Phi_m(-ia\tau_0 J_1(\xi a)\cos\theta)e^{i\xi(x\cos\theta+y\sin\theta)}\xi d\xi d\theta \tag{10}$$

Changing limits for θ, we get

$$u(r,\theta,\omega) = \frac{1}{4\pi^2}\int_{0}^{2\pi}\int_{-\infty}^{+\infty}\sum_{m=1}^{M}\frac{\hat{V}_m^L P_1}{(\xi_m-\xi)\hat{V}_m^L P\hat{V}_m^R}\Phi_m(-ia\tau_0 J_1(\xi a)\cos\theta)e^{i\xi(x\cos\theta+y\sin\theta)}\xi d\xi d\theta \tag{11}$$

Taking constant terms out of integral,

$$u(r,\theta,\omega) = \frac{-ia\tau_0}{4\pi^2}\int_{0}^{2\pi}\int_{-\infty}^{+\infty}\sum_{m=1}^{M}\frac{\hat{V}_m^L P_1}{(\xi_m-\xi)\hat{V}_m^L P\hat{V}_m^R}\Phi_m(J_1(\xi a)\cos\theta)e^{i\xi(x\cos\theta+y\sin\theta)}\xi d\xi d\theta \tag{12}$$

$$u(r,\theta,\omega) = \frac{-ia\tau_0}{4\pi^2}\int_{-\infty}^{\infty}\int_{0}^{\pi}\sum_{m=1}^{M}\frac{\hat{V}_m^L P_1}{(\xi_m-\xi)\hat{V}_m^L P\hat{V}_m^R}\Phi_m\xi(J_1(\xi a))e^{i\xi(x\cos\theta+y\sin\theta)}\cos\theta d\theta d\xi \tag{13}$$

Without loss of generality due to axisymmetry, consider the point $x = r, y = 0$. We substitute this point in to eq.(13). The following formula for Bessel function can then be used:

$$J_1(z) = \frac{-1}{\pi i}\int_{0}^{\pi} e^{i\xi z\cos\theta}\cos\theta d\theta \tag{14}$$

Hence we integrate eq.(13) into the following form

$$u(r,\omega) = \frac{a\tau_0}{4\pi}\int_{-\infty}^{+\infty}\sum_{m=1}^{M}(J_1(\xi a))\frac{\hat{V}_m^L P_1}{(\xi_m-\xi)\hat{V}_m^L P\hat{V}_m^R}\Phi_m J_1(\xi r)\xi d\xi \tag{15}$$

Applying residue theorem for integrating eq.(15), we get the expression for displacement field as following

$$u(r,\omega) = \frac{-ia\tau_0}{2}\sum_{m=1}^{M}(J_1(\xi_m a))\frac{\hat{V}_m^L P_1}{\hat{V}_m^L P\hat{V}_m^R}\Phi_m\xi_m J_1(\xi_m r) \tag{16}$$

Substituting $J_1(\xi_m r)$ in terms of Hankel functions, we get

$$u(r,\omega) = \frac{-ia\tau_0}{4}\sum_{m=1}^{M}(J_1(\xi_m a))\frac{\hat{V}_m^L P_1}{\hat{V}_m^L P \hat{V}_m^R}\Phi_m \xi_m (H_1^{(2)}(\xi_m r) + H_1^{(1)}(\xi_m r)) \tag{17}$$

Where $H_1^{(1)}(z)$ and $H_1^{(2)}(z)$ are the complex Hankel functions of order 1 and the first and second kinds, respectively, in the generic variable z . From far-field expressions, Hankel function of the first type corresponds to the inward propagation wave (assuming only the positive roots are retained in the contour for residue evaluation) while Hankel function of the second type corresponds to the outward propagation wave. Physically, hence the Hankel function of second type only makes sense. Thus, the final solution becomes,

$$u(r,\omega) = \frac{-ia\tau_0}{4}\sum_{m=1}^{M}(J_1(\xi_m a))\frac{\hat{V}_m^L P_1}{\hat{V}_m^L P \hat{V}_m^R}\Phi_m \xi_m (H_1^{(2)}(\xi_m r)) \tag{18}$$

For far field approximation, the following asymptotic expression hold for the Hankel function

$$\lim_{\xi r\to\infty} H_1^2(\xi r) = -\sqrt{\frac{1}{\pi\xi r}}(1+i)e^{i\xi r} \tag{19}$$

Substituting eq.(19) in to eq.(18), we get

$$u(r,\omega) = \frac{ia\tau_0}{4}\sum_{m=1}^{M}(J_1(\xi_m a))\frac{\hat{V}_m^L P_1}{\hat{V}_m^L P \hat{V}_m^R}\Phi_m \xi_m (\sqrt{\frac{1}{\pi\xi_m r}}e^{i\xi_m r}) \tag{20}$$

The in plane strain in radial direction can be derived from eq.(20) from the following strain displacement relation

$$\varepsilon_r(r,t) = \frac{\partial u_r(r,t)}{\partial r} \tag{21}$$

Hence from the radial displacement field the strain ε_r can be obtained as following

$$\varepsilon_r(r,\omega) = \frac{\partial}{\partial r}\left(\frac{ia\tau_0}{4}\sum_{m=1}^{M}(J_1(\xi_m a))\frac{\hat{V}_m^L}{\hat{V}_m^L P \hat{V}_m^R}\Phi_{mr}(\sqrt{\frac{\xi_m}{\pi r}}e^{i\xi_m r})\right) \tag{22}$$

After differentiation of eq.(22), we get the closed form expression for strain wave solution for plate upper surface ε_r as following

$$\varepsilon_r(r,\omega) = \frac{ia\tau_0}{4}\sum_{m=1}^{M}(J_1(\xi_m a))\frac{\hat{V}_m^L}{\hat{V}_m^L P \hat{V}_m^R}\Phi_{mr}(\xi_m^{3/2}\sqrt{\frac{1}{\pi r}}e^{i\xi_m r}) \tag{23}$$

3.2 SAFE-NME prediction of lamb wave propagation in hollow cylinder

This section compares the numerical simulation of theoretical expressions with the results of experiments conducted on hollow for validation of the theoretical expression derived in section 3.3. An excitation is applied at SG5 location of the hollow cylinder by using PWAS, at a frequency of 380 kHz. Response is collected at TF1 location of the cylinder using another PWAS. The signal received at TF1 is presented in Figure 4. SAFE-NME in eq.(23) for in-plane motion is used for predicting the lamb wave propagation in plate. The hollow cylinder is assumed to be constructed by a plate, which is wrapped around (wrapped plate approximation of hollow cylinder). The number of guided wave modes in a plate depends on the frequency and half-thickness product (fd). For the propagating, wave modes only the real part of the wavenumber has been considered. The phase velocity and group velocity dispersion curves for the Lamb waves are plotted in Figure 5. Both symmetric and antisymmetric Lamb wave modes are presented here.

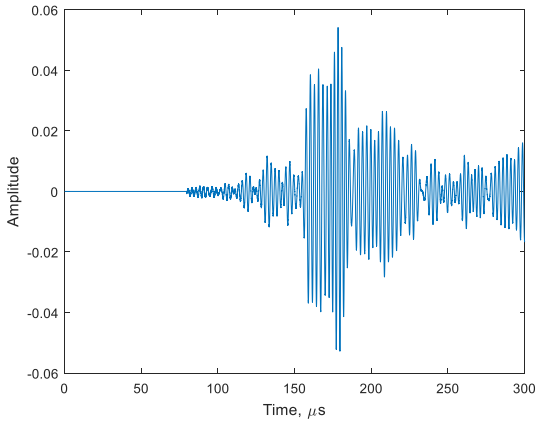

Figure 4 Response collected at TF1 due to an excitation at SG5

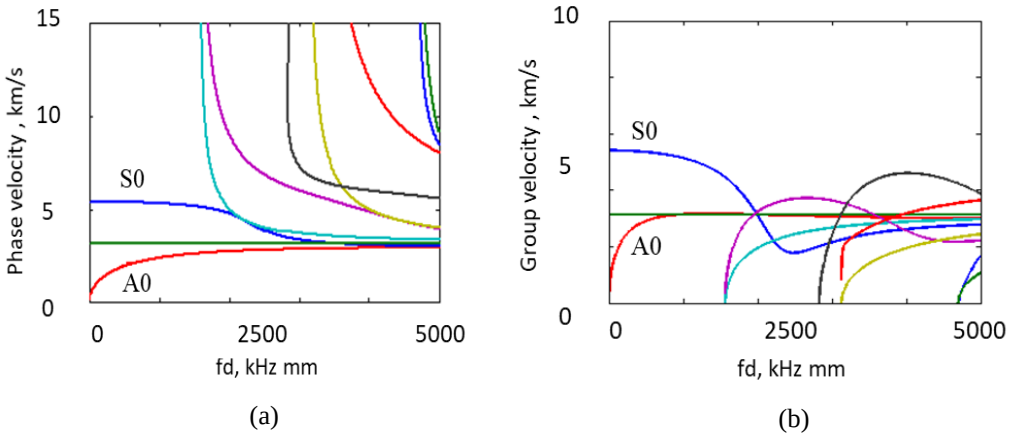

Figure 5 Dispersion curved for propagating Lamb wave modes: (a) phase velocity (b) group velocity

S0 and A0 plate modes only are considered for predictive modeling at this stage. A 3D prediction of S0 and A0 lamb wave modes and comparison of predicted signal with experimentally obtained signal is presented in Figure 6a.

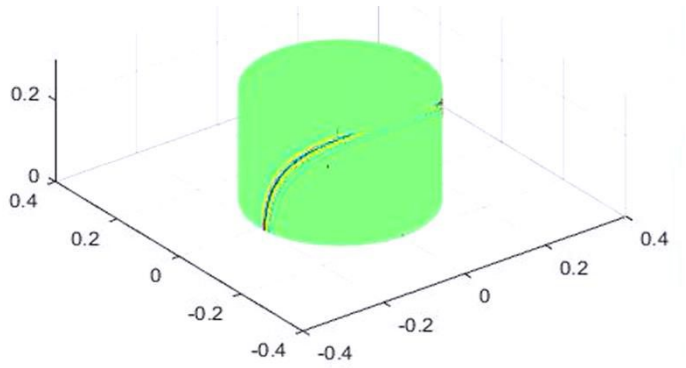

(a)

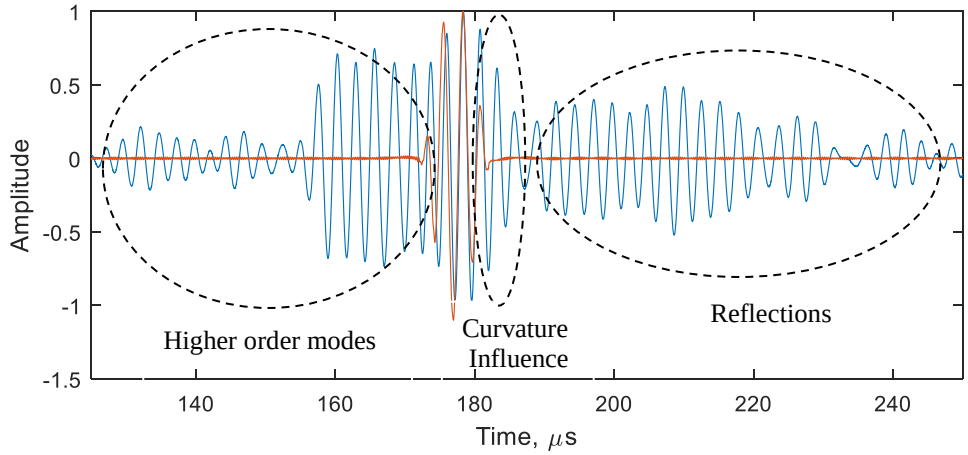

(b)

Figure 6 Wrapped plate approximation prediction of guided wave propagation in hollow cylinder a) 3D visualization b) Comparison of prediction with experiment

Figure 6b represents the comparison of experimentally obtained signal collected using PWAS at TF1 location and prediction of S0 and A0 signal at TF1 location using SAFE NME approach and wrapped plate approximation of cylinder. The presence of higher order modes can be detected before the arrival of S0 and A0 mode. Due to curvature effects minute deviation in experiment and prediction can be observed when the signals overlap. Due to the presence of curvature, higher order circumferential modes of the hollow cylinder which possess small variations in the phase velocities changes the spreading of S0 and A0 modes in the real signal. We can also observe the reflected waves after S0 and A0 modes.

4. EFFECT OF VARIOUS JOINTS IN THE STRUCTURE ON WAVE PROPAGATION

A broad class of wave propagation paths for the waveforms to reach the sensors in the hollow cylinder scaled down model is roughly identified as three. The first path is due to an excitation in the surface of the cylinder, reaching the sensors propagating through the cylinder, without any interruption (path 1). The second one starts from inside the basket guides travelling through the adhesive and bolted joints reaching the shell and finally reaching the sensors (path 2). The third path is due to an excitation in the trunnions travelling through the press fit joints, entering the cylinder, and reaching the sensors (path 3). For the paths 1 and 2, since there is presence of joints in the wave propagation paths due to adhesive or press fit, damping of the waveforms are expected. This section will study the effect of path1, path2 and path3 on the waveforms reaching the sensors.

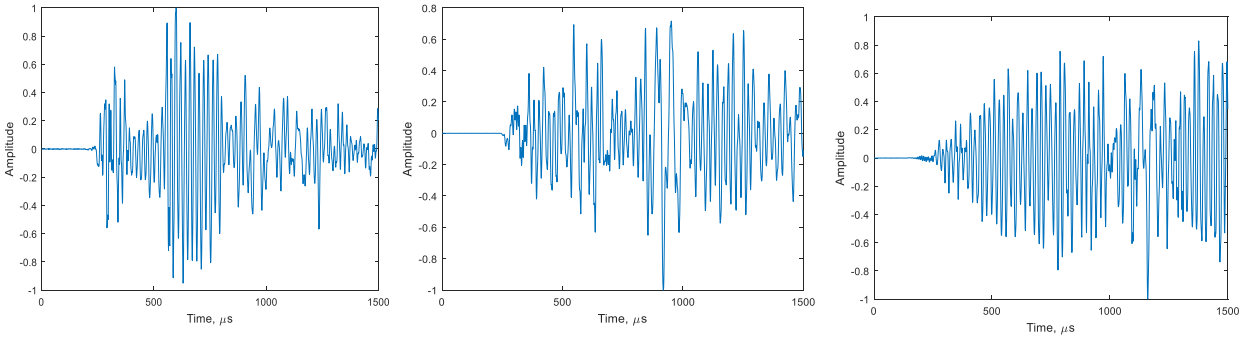

(a) (b) (c)

Figure 7 The signals received at R15α at face near T1 through various wave propagation paths. a) Path 1- excitation at BG1 b) Path 2- excitation at T1 c) Path 3- excitation at S1

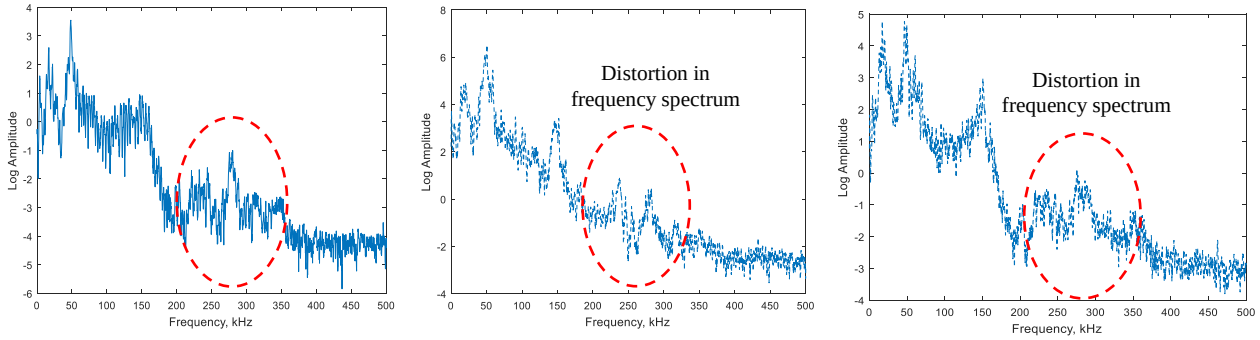

(a) (b) (c)

Figure 8 Frequency spectrum of waveforms received at R15α at face near T1 through various wave propagation paths. a) Path 1- excitation at BG1 b) Path 2- excitation at T1 c) Path 3- excitation at S1

Figure 8 compares the frequency spectrum of waveform received at R15α sensor at flat face near trunnion 1 through path 1, path 2 and path 3 respectively due to hammer hit excitations at S1, BG1 and T1 respectively. From the frequency plots, it observes that the major change in the frequency spectrum happens at higher frequencies. For excitation at S1 case (Path1), where the waves travels without any interference of joints, two frequency peaks between 200 to 300 kHz is visible. Whereas this peak shows some variation in the case of path 2, in which the waves travel through adhesive joints and bolted joints. The same peak is even more distorted in the case of path 3, in which the waves travel through the press fit. We may note the point here that the press fit joints shows higher magnitude of distortion higher frequency range than compared to adhesive joints. The distortions in the lower frequency for frequency spectrum are less in comparison to higher frequencies. Therefore, we may note the second point that the presence of joint shows distortions in the frequency spectrum majorly in higher frequency.

One of the characteristic of hammer-hit excitation is, it possess a higher magnitude of excitation for lower frequency range (below 100 kHz approximately) and possess lower excitability for higher frequencies above 100 kHz (approximately). This is a common observation from hammer excitation by a human being. Which makes it deliver a higher frequency response in low frequency range. To get a higher excitation in higher frequency range, we adopted pencil lead break excitation as reproducible AE source. R15α sensor is a resonant type sensor, which is having a resonance frequency of 150 kHz. It hardly picks up higher frequency excitations. Instead, WSα AE sensor has a wide band frequency response, responding to frequencies at even at 600 to 800 kHz range. Therefore, WSα with pencil lead break excitation will be a good exciter sensor combination to get the information's in higher frequency range.

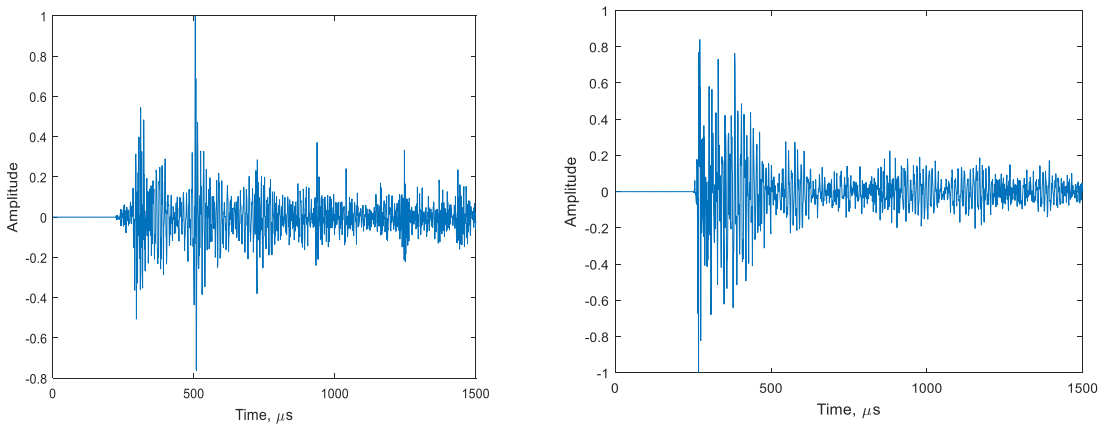

(a) (b)

Figure 9 Waveforms received at WSα at face near T1 through various wave propagation paths a) Through path 1 due to an excitation at S1 b) Through path 3 due to an excitation at T1

Figure 9 shows the waveforms received at WSα sensor through path 2 and path 3. Again, it is difficult to compare the waveforms to note the difference in paths. So logarithmic FFT of the signals are taken.

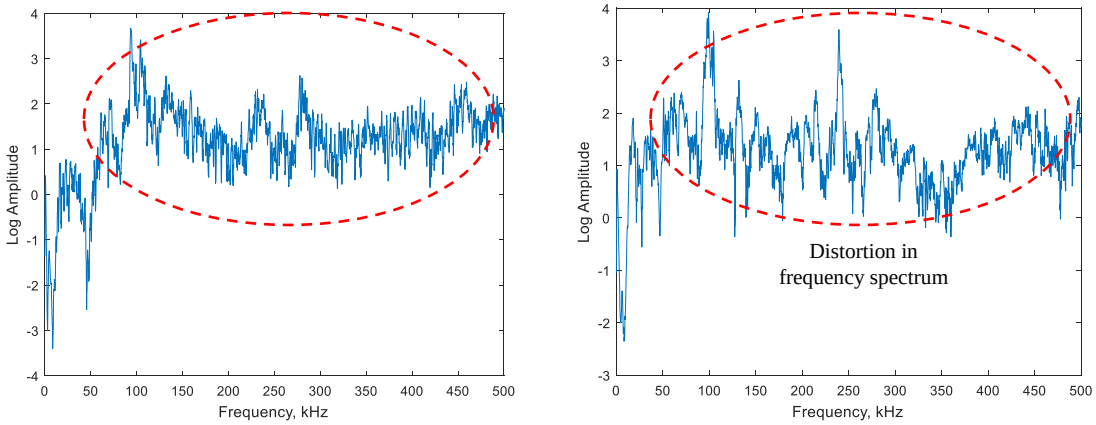

(a) (b)

Figure 10 Frequency spectrum of waveforms received at WSα at face near T1 through various wave propagation paths a) Through path 1 due to an excitation at S1 b) Through path 3 due to an excitation at T1

Figure 10 compares the frequency spectrum of waveform received at WSα sensor. At higher frequencies over a wide range, we can observe the change in peaks and valleys of the frequency response, due to difference in path. It is difficult to find out a most sensitive frequency. However, the overall frequency spectrum is distorted for two paths. At this situation, a point to be noted is, for R15α sensor, the higher frequency peaks were few and it was very easy to compare a peak for two paths. So, R15α is found to be more useful for frequency spectrum comparison at higher frequencies.

5. STUDY OF CHIRP EXCITATION AND FREQUENCY RESPONSE OF THE CASK

In order to get the frequency response of the hollow cylinder model, chirp excitations are given using PWAS transducers. The frequency range of the chirp was chosen to be from 30 kHz to 500 kHz. The hollow cylinder is excited at different locations using PWAS. The response signal is collected at face near trunnion 1 (TF1) and the FFT of the signal is taken to get the frequency response. Frequency response of waves travelling through path 1, path 2 and path 3 are processed. This section discusses on influence of wave propagation paths on frequency response spectrum due to chirp excitation.

Chirp excitation is given at S1 location and corresponding response measurement is done at TF1 location (path 1). FFT of the response signal gives frequency response, which is presented in Figure 11. Maximum frequency response is observed at approximately 320 to 380 kHz. Relatively high magnitude of frequency response is observed from frequencies 150 kHz to 400 kHz. A drastic change in frequency response was observed at 400 kHz.

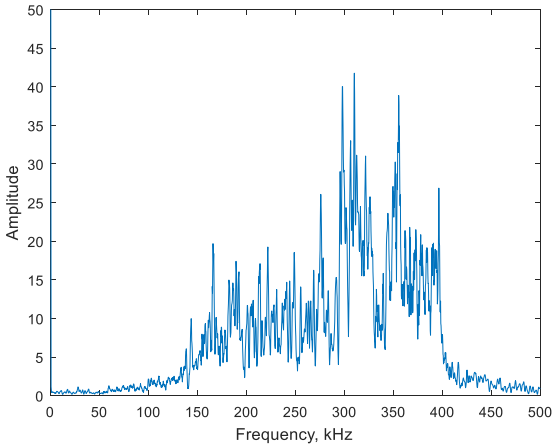

Figure 11 Frequency response of the hollow cylinder measured at PWAS glued to face near Trunnion 1 (TF1)

The basket is inserted into the hollow cylinder and the lid is screwed to the hollow cylinder. Frequency response is measured experimentally at TF1 by exciting PWAS at S1 using chirp (path 1). The frequency response is presented in Figure 12. The highest peak is found to remain the same. But the responses at other frequencies are found considerably changing compared to basket out case. A considerable change in frequency response is observed at frequencies above 320 kHz.

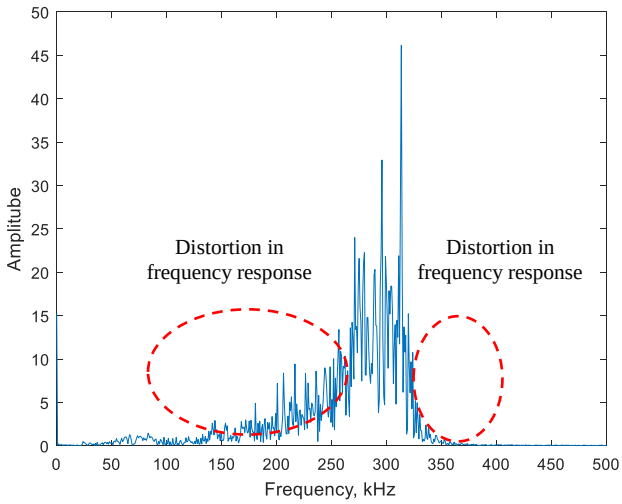

Figure 12 Frequency response measured at TF1 after inserting basket

The waves travel from the cylinder through the press fit joint to the trunnion. This is identical to the path 3 which is discussed in the previous section. A change in the frequency response is expected at a sensor placed at trunnion, since the waves are travelling through the joint. Frequency response calculated after doing FFT of waveform reaching PWAS at trunnion 1 is shown in Figure 13. Peaks and valleys of Figure 13 remains same as that of Figure 11. Even though, a change in amplitude of the frequency response is observed. The amplitude of the frequency response is found to reduce possibly due to the effect of press fit joint.

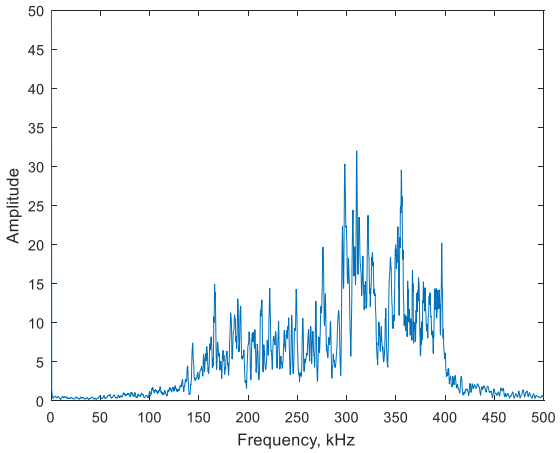

Figure 13 Frequency response measured at PWAS glued to Trunnion 1 (T1)

SUMMARY AND CONCLUSION

This paper presents the inspection of scaled down model of TN32 cask for health monitoring and understanding the guided wave propagation in the model. Numerical prediction of guided wave propagation in hollow cylinder scaled down model using SAFE-NME approach is done for the scaled down model and is validated with experimentally obtained data. The deviation from predicted plate guided waves due to the curvature effect is observed in the experimentally measured signal. It is hypothesized that the deviation of numerical prediction by assuming wrapped plate approximation of hollow cylinder from experimental measurement is due to the evasion of non-axisymmetric circumferential modes of hollow cylinder in the theoretical predictions.

Passive and active excitation and sensing of signals on hollow cylinder is done by using various AE sensors such as R15α and WSα sensors and PWAS. The joints in the cask are found sensitive to frequencies from 200 to 350 kHz. This frequency range will be very useful while passive sensing in real TN32 cask to distinguish the location of the origin of signals received. Frequency sweep excitation is applied on the hollow cylinder using PWAS to find the most sensitive frequency of the hollow cylinder. The hollow cylinder is found to be very sensitive to frequencies from 320 to 380 kHz. The frequency response of the cask due to in-plane excitation using PWAS is found to change with installation of the cask lid.

REFERENCES

[1] D. C. Gazis, “Exact Analysis of the Plane-strain Vibrations of Thick-walled Hollow Cylinders,” *J. Acoust. Soc. Am.*, vol. 30, pp. 786–794, 1958.

[2] J. J. Ditri and J. L. Rose, “Excitation of guided elastic wave modes in hollow cylinders by applied surface tractions,” *J. Appl. Phys.*, vol. 72, no. 7, pp. 2589–2597, 1992.

[3] J. Li and J. L. Rose, “Excitation and propagation of non-axisymmetric guided waves in a hollow cylinder,” *J. Acoust. Soc. Am.*, vol. 109, no. 2, pp. 457–464, 2001.

[4] Z. Sun, L. Zhang, and J. L. Rose, “Flexural Torsional Guided Wave Mechanics and Focusing in Pipe,” *J. Press. Vessel Technol.*, vol. 127, no. 4, p. 471, 2005.

[5] A. M. Kamal, B. Lin, and V. Giurgiutiu, “Exact analytical modeling of power and energy for multimode lamb waves excited by piezoelectric wafer active sensors,” *J. Intell. Mater. Syst. Struct.*, vol. 25, no. 4, pp. 452–471, 2014.

[6] B. Lin, M. Gresil, A. Cuc, and V. Giurgiutiu, “Predictive modeling of piezoelectric wafer active sensors for structural health monitoring,” *Ferroelectrics*, vol. 470, no. 1, pp. 168–182, 2014.

[7] Y. Shen and V. Giurgiutiu, "WaveFormRevealer: An analytical framework and predictive tool for the simulation of multi-modal guided wave propagation and interaction with damage," *Struct. Heal. Monit.*, vol. 13, no. 5, pp. 491–511, 2014.

[8] M. F. Haider and V. Giurgiutiu, "A Helmholtz Potential Approach to the Analysis of Guided Wave Generation During Acoustic Emission Events," *J. Nondestruct. Eval. Diagnostics Progn. Eng. Syst.*, vol. 1, no. 2, p. 21002, 2017.

[9] M. F. Haider and V. Giurgiutiu, "Analysis of axis symmetric circular crested elastic wave generated during crack propagation in a plate: A Helmholtz potential technique," *Int. J. Solids Struct.*, vol. 134, pp. 130–150, 2017.

[10] R. Joseph, M. Y. Bhuiyan, and V. Giurgiutiu, "Acoustic emission source modeling in a plate using buried moment tensors," *Proc. SPIE (Health Monit. Struct. Biol. Syst.*, vol. 10170, no. May, pp. 1017028-1–8, 2017.

[11] M. Y. Bhuiyan, B. Lin, and V. Giurgiutiu, "Acoustic emission sensor effect and waveform evolution during fatigue crack growth in thin metallic plate," *J. Intell. Mater. Syst. Struct.*, p. Accepted, 2017.

[12] M. J. Quarry and J. L. Rose, "Multimode Guided Wave Inspection of Piping Using Comb Transducers," *Mater. Eval.*, vol. 57, no. 10, pp. 1089–1090, 1999.

[13] D. N. A. and P. Cawley, "Long Range Propagation of Lamb Waves in Chemical Plant Pipework," *Mater. Eval*, vol. 45, no. 4, pp. 504–508, 1997.

[14] D. N. A. and P. Cawley, "The excitation of Lamb Waves in Pipes Using Dry-coupled Piezoelectric Transducers," *J. Nondestruct. Eval.*, vol. 15, no. 1, pp. 11–20, 1996.

[15] T. Hayashi, K. Kawashima, Z. Sun, and J. L. Rose, "Analysis of flexural mode focusing by a semianalytical finite element method.," *J. Acoust. Soc. Am.*, vol. 113, no. 3, pp. 1241–1248, 2003.

[16] S. B. Dong and R. B. Nelson, "On Natural Vibrations and Waves in Laminated Orthotopic Plates," *J. Appl. Mech.*, no. July, pp. 739–745, 1972.

[17] S. B. D. K.H. Huang, "Propagating waves and edge vibrations in anisotropic composite cylinders," *J. Sound Vib.*, vol. 96, no. 3, pp. 363–379, 1984.

[18] K. H. H. S.B. Dong, "Edge vibrations in laminated composite plates," *J. Appl. Mech.*, vol. 41, pp. 322–327, 1985.

[19] a C. Hladky-Hennion, "Finite element analysis of the propagation of acoustic waves in waveguides," *J. Sound Vib.*, vol. 194, no. 2, pp. 119–136, 1996.

[20] L. Gavrić, "Computation of propagative waves in free rail using a finite element technique," *J. Sound Vib.*, vol. 185, no. 3, pp. 531–543, 1995.

[21] X. Han, G. R. Liu, Z. C. Xi, and K. Y. Lam, "Characteristics of waves in a functionally graded cylinder," *Int. J. Numer. Methods Eng.*, vol. 53, no. 3, pp. 653–676, 2002.

[22] G. R. Liu, K. Y. Dai, X. Han, and T. Ohyoshi, "Dispersion of waves and characteristic wave surfaces in functionally graded piezoelectric plates," *J. Sound Vib.*, vol. 268, no. 1, pp. 131–147, 2003.

[23] E. Taciroglu, C. W. Liu, S. B. Dong, and C. K. Chun, "Analysis of laminated piezoelectric circular cylinders under axisymmetric mechanical and electrical loads with a semi-analytic finite element method," *Int. J. Solids Struct.*, vol. 41, no. 18–19, pp. 5185–5208, 2004.

[24] S. Finnveden, "Evaluation of modal density and group velocity by a finite element method," *J. Sound Vib.*, vol. 273, no. 1–2, pp. 51–75, 2004.

[25] I. Bartoli, A. Marzani, F. Lanza di Scalea, and E. Viola, "Modeling wave propagation in damped waveguides of arbitrary cross-section," *J. Sound Vib.*, vol. 295, no. 3–5, pp. 685–707, 2006.

[26] A. Marzani, E. Viola, I. Bartoli, F. Lanza di Scalea, and P. Rizzo, "A semi-analytical finite element formulation for modeling stress wave propagation in axisymmetric damped waveguides," *J. Sound Vib.*, vol. 318, no. 3, pp. 488–505, 2008.